ELSEVIER

Chemical Engineering Science 62 (2007) 4214–4228

Chemical Engineering Science

www.elsevier.com/locate/ces

Dynamics of a solar thermochemical reactor for steam-reforming of methane

Jörg Petrasch[a], Aldo Steinfeld[a,b,*]

[a]*Department of Mechanical and Process Engineering, ETH Zurich, 8092 Zurich, Switzerland*
[b]*Solar Technology Laboratory, Paul Scherrer Institute, 5232 Villigen, Switzerland*

Received 19 March 2007; accepted 25 April 2007

Abstract

A nonlinear dynamic model is developed for a steam/methane-reforming reactor that uses concentrated solar radiation as the source of high-temperature process heat. The model incorporates a set of lumped-parameter reservoirs for mass and energy. For each reservoir, the unsteady mass and energy conservation equations are formulated, which couple conduction, convection, and radiation heat transfer with the temperature dependent chemical conversion. Radiative exchange, the dominant heat transfer mode at above 800 K, is solved by a band-approximation Monte Carlo technique. The dynamic model is applied to predict the transient behavior of a 400 kW prototype solar reformer in operational modes of purging, thermal testing, startup, chemical reaction, shutdown, and cyclical operation. Time constants vary between 2 s for species transport and 1×10^5 s for thermal energy transport through ceramic insulation. Validation is accomplished by comparing modeled and experimentally measured outlet gas temperatures obtained from reactor tests in a solar tower facility.

Keywords: Dynamic simulation; Solar reactor; Solar reforming; Radiation; Heat transfer; Porous media

1. Introduction

Solar reforming processes, in which hydrocarbons are used exclusively as the chemical source for syngas production and concentrated solar radiation, is used exclusively as the energy source of process heat, offer a viable route for fossil fuel decarbonization, and create a transition path towards solar hydrogen (Steinfeld, 2005). Solar reforming using either H_2O or CO_2 as partial oxidant has been extensively studied in solar concentrating facilities with small-scale solar reactor prototypes using Rh-based catalyst (Levy et al., 1989, 1992; Hogan et al., 1990; Richardson and Paripatyadar, 1990; Buck et al., 1991, 1994; Wörner and Tamme, 1998) and Fe-based catalysts (Kodama et al., 2001; Gokon et al., 2002), and without added catalysis (Dahl et al., 2004). The solar reforming process has been scaled-up to a power level of 400 kW and tested at 1100 K and 8–10 bar in a solar tower concentrating system using two solar reforming reactor concepts: an indirect-irradiation tubular reactor (Epstein and Spiewak, 1996) and a direct-irradiation volumetric reactor (Tamme et al., 2001; Moeller et al., 2002). The latter is being further developed within the EU-project SOLREF (http://www.solref.dlr.de/). The chemical thermodynamics and process engineering of solar reforming under the operating conditions of the 400 kW demonstration plant have been examined, and a steady-state process model that includes mass/energy conservation coupled to chemical equilibrium composition is formulated to predict the system steady-state performance of an idealized and the 400 kW-demonstration solar reforming plant (Petrasch et al., 2005). System optimization predicts a peak solar-to-chemical energy conversion efficiency of 60%.

Due to the inherently transient nature of solar irradiation, the dynamic behavior of the solar reforming plant is critical for its efficient and safe operation. Previous pertinent papers on the dynamics of solar thermal systems include studies on flat plate solar collectors (De Ron, 1980; Hashish and El-Refaie, 1983; Jallut et al., 1988; Arinze et al., 1993; Chaabene and Annabi, 1997; Buzás et al., 1998); solar steam generation

* Corresponding author. Department of Mechanical and Process Engineering, ETH Zurich, 8092 Zurich, Switzerland. Tel.: +41 44 6327929; fax: +41 44 6321065.
E-mail address: aldo.steinfeld@eth.ch (A. Steinfeld).

0009-2509/$ - see front matter © 2007 Elsevier Ltd. All rights reserved.
doi:10.1016/j.ces.2007.04.036

Please cite this article as: Petrasch, J., Steinfeld, A., Dynamics of a solar thermochemical reactor for steam-reforming of methane. Chemical Engineering Science (2007), doi: 10.1016/j.ces.2007.04.036

Nomenclature

A	area, m; absorptance, dimensionless
c_p	mass specific heat at constant pressure, J/kg K
$\bar{c}_p$	mole specific heat at constant pressure, J/mol K
c_v	mass specific heat at constant volume, J/kg K
$D_{i,j,k}$	Band-averaged spectral radiation distribution factor, dimensionless
F_k	blackbody fractional function for band k, dimensionless
h	mass specific enthalpy, J/kg
$\bar{h}$	molar specific enthalpy, J/mol
$\bar{h}_{\text{conv}}$	average convection heat transfer coefficient, $\text{W}/(\text{m}^2\,\text{K})$
$H_{i,k}$	fraction of solar energy in band k absorbed in segment j, dimensionless
k	thermal conductivity, W/(m K); imaginary part of complex refractive index, dimensionless
l	length, m
m	mass, kg
$\dot{m}$	mass flow rate, kg/s
n	number of moles, mol; real part of the complex refractive index, dimensionless
$\dot{n}$	molar flow rate, mol/s
Nu	Nusselt number, dimensionless
p	pressure, Pa
Pr	Prandtl number, dimensionless
Q	thermal power, W
Q_{solar}	solar input power, W
R	reflectance, dimensionless
$\bar{R}$	ideal gas constant, J/(mol K)
Ra	Rayleigh number, dimensionless
Re	Reynolds number, dimensionless
T	temperature, K; transmittance, dimensionless
V	volume, m^3
y	molar fraction, dimensionless

Greek letters

ε	emissivity, dimensionless
η	efficiency, dimensionless
θ	angle of incidence of radiation on quartz window, deg
κ	absorption coefficient, 1/m
λ	wavelength, μm
ρ	reflectivity, dimensionless
τ	time constant, s; transmittance along one pass through window, dimensionless
χ	angle of diffracted radiation, deg

Subscripts

c	ceramic insulation
cond	conduction
conv	convection
en	energy
g	gas
i	counter for reactor components and cavity surfaces
if	interface
in	in
ins	inside
j	counter for species; counter for reactor components and cavity surfaces
k	counter for wavelength bands
loss	loss
out	out
outs	outside
p	porous absorber
r	gas receiver
rad	radiation
s	solid
solar	solar
∞	surroundings

Abbreviations

C	cavity
I	insulation
P	porous absorber
R	gas receiver
S	separator
W	quartz window

(Ray, 1980, 1981; Maffezzoni and Parigi, 1982a, b), solar heating (Al-Nimr and Damseh, 1998), solar refrigeration (Kaushik et al., 1985, 1991), and concentrated solar heating in space applications (Cui et al., 2003). Widely used is the software package TRNSYS, which allows for dynamic simulation of conventional solar components and systems, but cannot handle solar thermochemical processes that involved coupled mass/heat transport of reactive flows. The dynamics of reforming reactors have been studied for small-scale mobile applications (Robbins et al., 2003; Beckhaus et al., 2004). In this paper, a detailed dynamic model is developed for the 400 kW solar reformer and applied to simulate its transient behavior during purging, thermal testing, startup, chemical reaction, and shutdown. Simulation results are presented in terms of the time-variation of temperatures, heat transfer rates, outlet flow rate, and product chemical composition. Validation is accomplished by comparing with experimentally measured data obtained from reactor tests in a solar tower facility.

2. Model formulation

Methodology—The modeling methodology follows approaches described by Guzzella (2001), Luyben (1989), and Bequette (1998, 2003). Special emphasis is devoted to

Please cite this article as: Petrasch, J., Steinfeld, A., Dynamics of a solar thermochemical reactor for steam-reforming of methane. Chemical Engineering Science (2007), doi: 10.1016/j.ces.2007.04.036

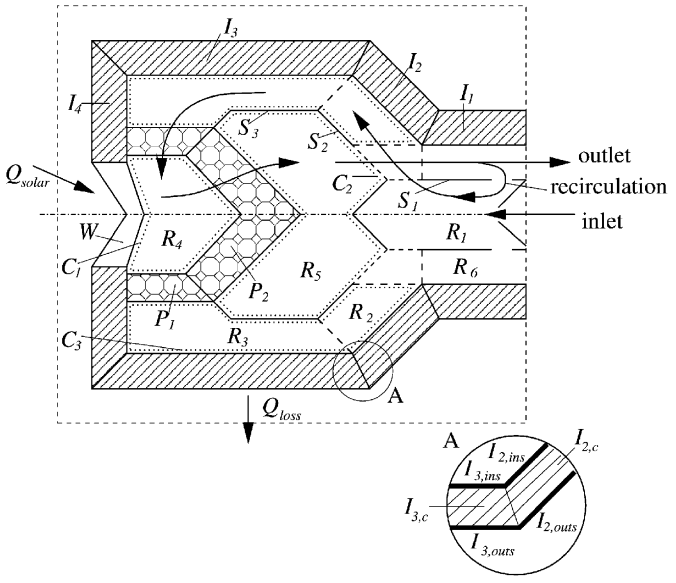

Fig. 1. Schematic representation of the 400 kW solar reforming reactor. Indicated are the lumped-parameter mass/energy reservoirs R, I, W, P, and S, and the system boundaries by the dashed rectangle.

establishing a nonlinear, physically based model of solar steam-reforming that is detailed enough to capture the relevant transient and steady-state characteristics of the dynamic system without parameter identification and with limited use of empirical parameters. It consists of the following steps: (a) the system domain is divided into a set of lumped-parameter reservoirs for mass and energy, for which the time constants are determined; (b) mass and energy conservation equations are formulated for each relevant reservoir; (c) algebraic relations for mass and energy transfer between individual reservoirs are derived; and (d) numerical algorithms are implemented and tested for typical operational modes.

(a) *System domain*: The system domain is defined by the dashed rectangle in Fig. 1. The axially symmetric reactor consists of an insulated cavity with a windowed aperture to let in concentrated solar energy. The cavity contains a catalytic porous absorber directly exposed to the incoming high-flux solar irradiation. The reacting gas, directed to the reactor front through passages defined by metal sheets, flows through the catalytic porous absorber where it undergoes reforming. The domain is divided into lumped-parameter mass and energy reservoirs, as indicated in Fig. 1. Reservoirs R_j are gas sub-volumes for energy and mass. Reservoirs I_j are thermal insulation segments, each subdivided into three concentric sub-elements $I_{j,\mathrm{ins}}$ (inner metal shell), $I_{j,c}$ (ceramic insulation), and $I_{j,\mathrm{outs}}$ (outer metal shell). Further types of thermal reservoirs are the quartz window W, the porous absorbers P_j (solid part only since mass and energy of the gas that fills the void fraction are negligible), and separators sheets S_j. Table 1 lists the estimated time constants of the reservoirs. They vary between 2 s for species transport in reactor volumes and 1×10^5 s for thermal energy in insulation. The gas flow dynamics are relatively fast and the pressure drops throughout the reactor are relatively small compared to the system pressure. Subsequently, the number of gas molecules contained in each receiver R_j is a static function of temperature and pressure of the respective reservoir. The gas species involved are assumed to obey the ideal gas law. The relevant time-scale of the process is taken as $2–1\times10^5$ s.

(b) *Conservation equations*: The general unsteady conservation equation for a generic reservoir is

$$\frac{\mathrm{d}[\text{reservoir content}]}{\mathrm{d}t}=\sum[\text{inflows}]-\sum[\text{outflows}]. \tag{1}$$

When applied for a solid element such as an insulation segment, the quartz window, or a separator, it yields

$$m_s c_{v,s}(T_s)\frac{\mathrm{d}T_s}{\mathrm{d}t}=\dot{Q}_{\mathrm{rad},s}+\sum_{\text{reservoir:}i}\dot{Q}_{\mathrm{conv},i\to s}+\sum_{\text{reservoir:}i}\dot{Q}_{\mathrm{cond},i\to s}-\dot{Q}_{\mathrm{conv},s\to\infty}. \tag{2}$$

The residence time of a gas molecule inside the void fraction of the porous absorbers is estimated at 0.7 s (Table 1). Thus, their mass balance is modeled as steady state. Further, solid–gas heat transfer rate at the porous absorber is fast enough to reasonably assume that the gas outlet temperature equals the solid temperature (Buck, 2002). Chemical equilibrium is attained as the reactant gas passes through the absorber (Buck, 2002). Neglecting kinetic and potential effects, the energy conservation equation for a porous absorber becomes

$$\frac{\mathrm{d}T_p}{\mathrm{d}t}\cdot m_p c_{v,p}(T_p)=\dot{n}_{g,\mathrm{in}}\sum_{\text{species:}j}y_{j,\mathrm{in}}\bar{h}_j(T_{\mathrm{in}})-\dot{n}_{g,\mathrm{out}}\times\sum_{\text{species:}j}y_{j,\mathrm{out}}\bar{h}_j(T_p)+\dot{Q}_{\mathrm{rad},p}+\sum_{\text{reservoir:}i}\dot{Q}_{\mathrm{cond},i\to p}. \tag{3}$$

The chemical equilibrium composition at temperature T_p, $y_{j,\mathrm{out}}$, is found by Gibbs free energy minimization. $\dot{n}_{g,\mathrm{out}}$ is computed from $\dot{n}_{g,\mathrm{in}}$ and composition via elemental conservation. The first two terms on the RHS of Eq. (3) contain both the reaction enthalpy change and the change in sensible heat of the gas passing through the absorber.

The gas volumes R_1–R_6 are modeled as continuously stirred without chemical reaction because the rate of the non-catalytic reaction is negligible compared to rate of the reaction with catalyst. Applying mass conservation to individual species and to the overall balance yields

$$\frac{\mathrm{d}n_{r,j}}{\mathrm{d}t}=\dot{n}_{\mathrm{in},j}-\dot{n}_{\mathrm{out},j}=y_{\mathrm{in},j}\dot{n}_{\mathrm{in}}-y_{r,j}\dot{n}_{\mathrm{out}}, \tag{4}$$

$$\frac{\mathrm{d}n_r}{\mathrm{d}t}=\dot{n}_{\mathrm{in}}-\dot{n}_{\mathrm{out}}. \tag{5}$$

Please cite this article as: Petrasch, J., Steinfeld, A., Dynamics of a solar thermochemical reactor for steam-reforming of methane. Chemical Engineering Science (2007), doi: 10.1016/j.ces.2007.04.036

Table 1
Estimated time constants τ for mass/energy reservoirs

Reservoir	Type	Reservoir content	Simplified, expression for τ	τ (s)
R_4	Gas volume	Energy	$\frac{n_{R4}\bar{c}_{p,\mathrm{gas}}}{\dot{n}\bar{c}_{p,\mathrm{gas}}+h_{\mathrm{conv}}A_{\mathrm{conv},R4}}$	2.2
		Gas dynamics	$\frac{V_{R4}\mu_{\mathrm{gas}}D_{\mathrm{porous}}}{R_{\mathrm{gas}}T_{\mathrm{gas}}K_{\mathrm{porous}}\rho_{\mathrm{gas}}A_{\mathrm{porous}}}$	3.5×10^{-6}
		Species	$\frac{n_{R4}}{\dot{n}}$	2.6
$I_{3,c}$	Solid	Energy	$\approx\frac{m_{I3c}c_{I3c}}{2A_{\mathrm{cond},I3c}\frac{k_{I3c}}{l_{I3c\to\mathrm{if}}}}$	4.5×10^{4}
$I_{3,i}$	Solid	Energy	$m_{I3i}c_{I3i}\Big/\left(\begin{array}{c}A_{\mathrm{cond},I3i}\frac{k_{I3i}}{l_{I3i\to\mathrm{if}}}\left(1-\frac{k_{I3i}/l_{I3i\to\mathrm{if}}}{k_{I3i}/l_{I3i\to\mathrm{if}}+k_{I3c}/l_{I3c\to\mathrm{if}}}\right)\\+A_{\mathrm{conv},I3i}h_{\mathrm{conv}}+4\sigma\varepsilon_{I3i}A_{\mathrm{rad},I3i}T_{i3i}^3\end{array}\right)$	66
Q	Solid	Energy	$m_qc_q\Big/\left(\begin{array}{c}A_{\mathrm{cond},q}\frac{k_q}{l_{q\to if}}\left(1-\frac{k_q/l_{q\to\mathrm{if}}}{k_q/l_{q\to\mathrm{if}}+k_{i4}/l_{i4\to\mathrm{if}}}\right)\\+A_{\mathrm{conv},q}h_{\mathrm{conv}}+2A_{\mathrm{rad},q}4\sigma\varepsilon_qT_q^3\end{array}\right)$	144
P_2	Porous absorber	Energy in solid	$m_pc_p\Big/\left(\begin{array}{c}A_{\mathrm{cond},p}\frac{k_p}{l_{p\to\mathrm{if}}}\left(1-\frac{k_p/l_{p\to\mathrm{if}}}{k_p/l_{p\to\mathrm{if}}+k_{s3}/l_{s3\to\mathrm{if}}}\right)\\+A_{\mathrm{conv},p}h_{\mathrm{conv},p}+2A_{\mathrm{rad},q}4\sigma\varepsilon_pT_p^3\end{array}\right)$	4.4
		Energy in gas	$\frac{n_{\mathrm{gas},p}\bar{c}_{p,\mathrm{gas}}}{A_{\mathrm{conv},p}h_{\mathrm{conv},p}}$	0.043
		Species in gas	$\frac{n_{\mathrm{gas},p}}{\dot{n}}$	0.7

Assumptions: fluid: steam at 10^6 Pa, ideal gas, $\bar{c}_{p,\mathrm{gas}}\approx42$ J/mol K, $\dot{n}\approx6.2$ mol/s, $h_{\mathrm{conv}}\approx20$ W/m^2 K, A_{conv}, $R_4=2.9$ m^2, $V_{R4}=0.14$ m^3, $\mu_{\mathrm{gas}}\approx3.4\times10^{-5}$ N s/m, $D_p=0.045$ m, $R_{\mathrm{gas}}=462$ J/kg K, $T_{\mathrm{gas}}=1000$ K, $k_p=6\times10^{-8}$ m^2, $A_p=1$ m^2, $m_{I3c}=96$ kg, $c_{I3c}=1000$ J/kg K, $A_{\mathrm{cond},I3c}=2.3$ m^2, $k_{i3c}=0.03$ W/m K, $l_{I3c\to\mathrm{if}}=0.07$ m, $A_{\mathrm{rad},I3i}=A_{\mathrm{conv},I3i}=A_{\mathrm{cond},I3i}=2.3$ m^2, $m_{I3i}=31$ kg, $c_{I3c}=550$ J/kg K, $k_{i3i}=23$ W/m K, $l_{I3i\to\mathrm{if}}=0.001$ m, $\varepsilon_{i3i}=0.8$, $T_{i3i}=800$ K; $m_q=24$ kg, $c_q=1120$ J/kg K, $k_q=2.2$ W/m K, $l_{q\to\mathrm{if}}=0.3$ m, $k_{i4}=23$ W/m K, $l_{i4\to\mathrm{if}}=0.06$ m, $A_{\mathrm{rad},q}=A_{\mathrm{conv},q}=1.4$ m^2, $A_{\mathrm{cond},q}=0.05$ m^2, $T_q=800$ K, $m_p=16$ kg, $c_p=1240$ J/kg K^{-1}, $k_p=0.29$ W/m K, $l_{p\to\mathrm{if}}=0.35$ m, $k_{s3}=23$ W/m K, $l_{s3\to\mathrm{if}}=0.001$ m, $A_{\mathrm{rad},p}=1$ m^2, $A_{\mathrm{conv},p}=51$ m^2, $h_{\mathrm{conv},p}\approx85$ W/m K, $A_{\mathrm{cond},p}=0.13$ m^2, $T_p=1100$ K, $n_{\mathrm{gas},p}=4.4$ mol.

Thus, assuming that the enthalpy of each species j is a function of temperature only (independent of pressure),

$$\frac{\mathrm{d}T_r}{\mathrm{d}t}\cdot\sum_{\text{species:}j}n_{r,j}\bar{c}_{p,j}(T_r)=\sum_{\text{species:}j}\dot{n}_{\mathrm{in},j}(\bar{h}_j(T_{in})-\bar{h}_{r,j}(T_r))+\sum_{\text{reservoir:}i}Q_{\mathrm{conv},i\to r}+\frac{\mathrm{d}p_r}{\mathrm{d}t}V_r. \tag{6}$$

(c) *Mass and energy transfer*: Interaction between the various reservoirs is given by mass and energy transfer. These interactions are illustrated in the causality diagram of Fig. 2, where each box symbolizes one or several reservoirs for mass and/or energy and arrows symbolize mass and energy flows between the reservoirs or between the reservoirs and the surroundings. Mass transfer is modeled static throughout the system. Assuming ideal gas, the number of moles inside each gas volume and its time derivative can be expressed as

$$n_r=\frac{p_rV_r}{\bar{R}T_r};\quad \frac{\mathrm{d}n_r}{\mathrm{d}t}=\frac{V_r}{\bar{R}}\left(\frac{\dot{p}_rT_r-p_r\dot{T}_r}{T_r^2}\right). \tag{7}$$

The molar inflow and outflow for each of the serially arranged gas volumes R_1–R_6 can be found by combining Eqs. (5) and (7).

Radiation—Under typical operation conditions at above 800 K, radiative exchange is the dominant mode of heat transfer. The READ method (Yang et al., 1995) extended to band-averaged spectral properties (Mahan, 2002) is applied. The solar chemical reactor is divided into three cavities C_1, C_2, and C_3, as shown in Fig. 1, each made up of a set of cavity walls. For example, C_1 is made up from all walls adjoining gas volume R_4, namely the window W, the porous absorbers P_1 and P_2, and parts of insulation I_4. Temperatures and optical properties of each individual wall are assumed uniform.

Please cite this article as: Petrasch, J., Steinfeld, A., Dynamics of a solar thermochemical reactor for steam-reforming of methane. Chemical Engineering Science (2007), doi: 10.1016/j.ces.2007.04.036

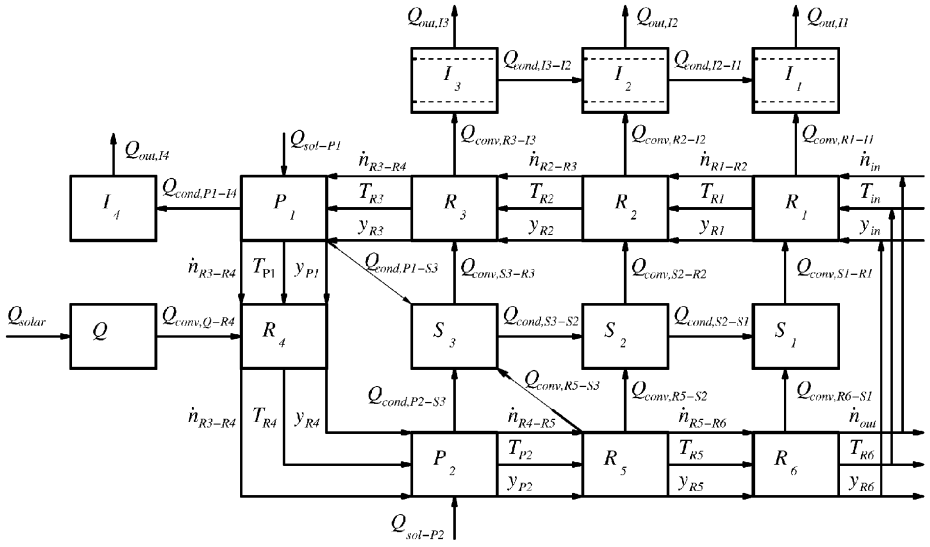

Fig. 2. Causality diagram for the solar steam-reforming reactor, without radiation exchange.

Optical properties are dependent on wavelength and angle of emitted and incident radiation; however, they are assumed independent of temperature. The directional-spectral transmittance, reflectance, and absorptance of the window W are given in terms of its surface's spectral-directional reflectivity ρ and its spectral transmittance along one pass through the window τ by

$$T_k = \tau\left[\frac{(1-\rho)^2}{1-\rho^2\tau^2}\right], \quad R_k = \rho\left[1+\frac{(1-\rho)^2\tau^2}{1-\rho^2\tau^2}\right],$$

$$A_k = \frac{(1-\rho)(1-\tau)}{1-\rho\tau}, \tag{8}$$

where

$$\kappa = \frac{4\pi k_{\text{quartz}}}{\lambda},$$

$$\tau = \mathrm{e}^{-\kappa d/\cos\chi},$$

$$\sin\chi/\sin\theta = n_\infty/n_{\text{quartz}},$$

$$\rho = \frac{1}{2}\frac{\sin^2(\theta-\chi)}{\sin^2(\theta+\chi)}\left[1+\frac{\cos^2(\theta+\chi)}{\cos^2(\theta-\chi)}\right]. \tag{9}$$

T_k, R_k, and A_k were calculated for the 8 mm thick plane layer of quartz, using Fresnel's and Beer's laws with the measured complex refractive index (Palik, 1985). They are plotted in Fig. 3 as a function of the angle of incidence for three spectral bands k: $\lambda < 0.15\,\mu\text{m}$, $0.15 \leqslant \lambda \leqslant 4\,\mu\text{m}$, and $\lambda > 4\,\mu\text{m}$. Classical collision-based Monte Carlo (MC) is used to obtain the band-averaged spectral radiation distribution factors $D_{i,j,k}$ for each

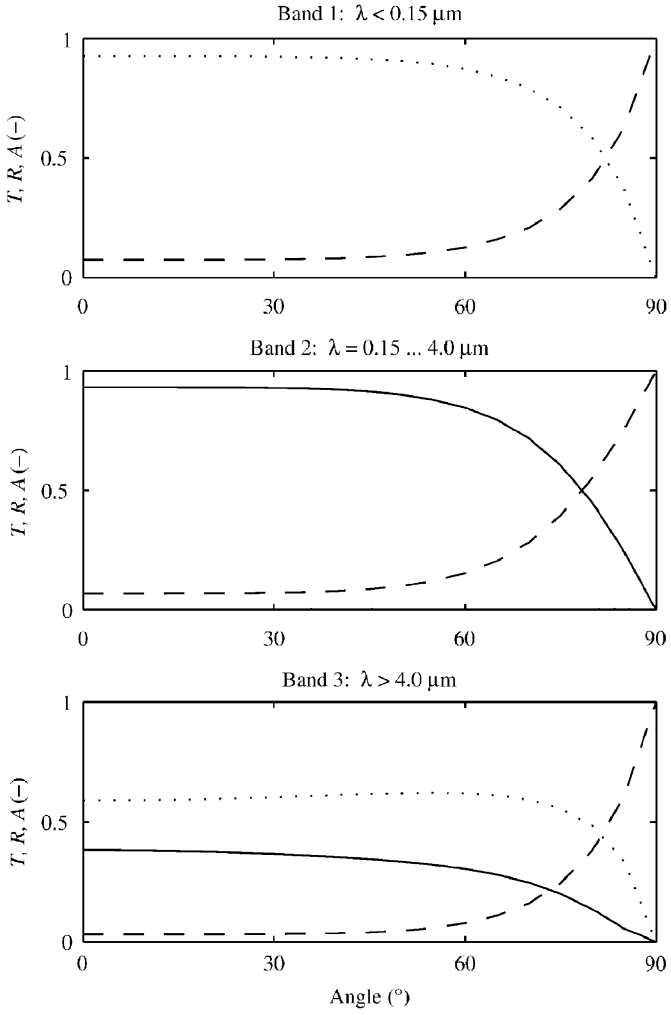

Fig. 3. Overall transmittance T (solid), reflectance R (dashed), and absorptance A (dotted) of a 8 mm quartz window as a function of angle of incidence for three wavelength bands: $\lambda < 0.15\,\mu\text{m}$, $0.15 \leqslant \lambda \leqslant 4\,\mu\text{m}$, and $\lambda > 4\,\mu\text{m}$. Note that $T = 0$ in band 1 (i.e., the window is opaque), whereas A approaches 0 in band 2 (only transmission and reflection).

Please cite this article as: Petrasch, J., Steinfeld, A., Dynamics of a solar thermochemical reactor for steam-reforming of methane. Chemical Engineering Science (2007), doi: 10.1016/j.ces.2007.04.036

Table 2
Convective heat transfer correlations

Flow type	Correlation	Reference	Reservoir pairs
Forced convection	$Nu_0 = \sqrt[3]{3.66^3 + 1.61^3\, Re\, Pr\, d_i/l}$	VDI (1984, p. Gb-1, Eqs. 2, 3, p. Gb-3, Eqs. 4–6)	$R_1 - S_1$
round, short	$Nu_0 = 0.664\sqrt[3]{Pr}\sqrt{Re\dfrac{d_i}{l}}$		
tube	$Nu = Nu_0\left(\dfrac{Pr}{Pr_w}\right)^{0.11}$		
	$Nu_0 = \dfrac{\xi/8(Re-1000)Pr}{1+12.7\sqrt{\xi/8}(Pr^{2/3}-1)}\left[1+\left(\dfrac{d_i}{l}\right)^{2/3}\right]$		
	$\xi = (1.82\log_{10}(Re) - 1.64)^{-2}$		
Free convection	$Nu = C\, Ra_{\mathrm{d}}^{\mathrm{n}}$	Incropera and DeWitt (1996, p. 465, Eq. 9.33)	$I_1 - \infty$, $I_2 - \infty$, $I_3 - \infty$
horizontal cylinder	*Ra* / *C* / *n*: 10^{-10}–10^{-2} / 0.675 / 0.058; 10^{-2}–10^{2} / 1.02 / 0.148; 10^{2}–10^{4} / 0.850 / 0.188; 10^{4}–10^{7} / 0.480 / 0.250; 10^{7}–10^{12} / 0.125 / 0.333		
Forced convection annular flow	$Nu = \left[Nu_\infty\, f\left(\dfrac{d_i}{d_o}\right)\dfrac{0.19\left(Re\,Pr\dfrac{d_h}{l}\right)^{0.8}}{1+0.117\left(Re\,Pr\dfrac{d_h}{l}\right)^{0.467}}\right]\left(\dfrac{Pr}{Pr_w}\right)^{0.11}$	VDI (1984, p. Gd-1, Eqs. 1, 4, 7)	$R_3 - S_3$, $R_3 - I_{3i}$, $R_6 - S_1$, $R_6 - I_1$
	$Nu_\infty = 3.66 + \left[4 - \dfrac{0.102}{(d_i/d_o + 0.02)}\right]\left(\dfrac{d_i}{d_o}\right)^{0.04}$		
	$f\left(\dfrac{d_i}{d_o}\right) = 1 + 0.14(d_i/d_o)^{0.1}$		
Forced convection flat plate	$Nu_l = 2\dfrac{0.3387Re_l^{1/2}Pr_l^{1/2}}{[1+(0.0468/Pr)^{2/3}]^{1/4}}$	Incropera and DeWitt (1996, p. 331,	R_2–S_2, R_2–I_{2i}, R_4–I_{4i},
	$Nu_l = (0.037Re_l^{4/5} - 871)Pr^{1/3}$	Eq. 7.27, p. 333, Eq. 7.33)	R_4–Q, R_5–S_2, R_5–S_3

Please cite this article as: Petrasch, J., Steinfeld, A., Dynamics of a solar thermochemical reactor for steam-reforming of methane. Chemical Engineering Science (2007), doi: 10.1016/j.ces.2007.04.036

Table 3
Geometrical properties for conduction calculations

Solid pair	Conduction length 1–2 (m)	Conduction length 2–1 (m)	Conduction cross-section (m^2)
I_{1c}–I_{2c}	0.5	0.2	0.1354
I_{1i}–I_{2i}	0.5	0.2	0.0012
I_{1o}–I_{2o}	0.5	0.2	0.0157
I_{2c}–I_{3c}	0.2	0.45	0.3437
I_{2i}–I_{3i}	0.2	0.45	0.0047
I_{2o}–I_{3o}	0.2	0.45	0.0377
I_{3c}–I_4	0.45	0.07	0.4639
I_{3i}–I_4	0.45	0.07	0.0047
I_{3o}–I_4	0.45	0.07	0.0377
I_{1i}–I_{1c}	0.00075	0.05	1.099
I_{1c}–I_{1o}	0.05	0.005	2.199
I_{2i}–I_{2c}	0.00075	0.05	0.809
I_{2c}–I_{2o}	0.05	0.005	1.068
I_{3i}–I_{3c}	0.00075	0.05	2.897
I_{3c}–I_{3o}	0.05	0.005	3.619
I_4–Q	0.06	0.3	0.0498
I_4–P_1	0.02	0.08	0.1335
I_{p1}–S_3	0.08	0.3	0.1335
S_3–P_2	0.3	0.35	0.1335
S_3–S_2	0.3	0.25	0.0155
S_2–S_1	0.25	0.5	0.0039

Table 4
Solid materials used and references to their physical properties

Material	Relevant property	Reference
Microtherm Insulation	Thermal conductivity	Microtherm International limited (2005)
	Specific heat	Microtherm International Limited (2005)
Inconel 600	Thermal conductivity	Special Metals Corporation (2000)
	Specific heat	Lucks et al. (1954)
	Emissivity (oxidized, inconel X)	Wood et al. (1964)
Quartz glass	Thermal conductivity	Touloukian et al. (1970)
	Specific heat	Scott (1962), Lucks et al. (1960), Van Lack (1964)
	Complex refractive index	Palik (1985)

cavity, defined as the fraction of energy emitted in band k from wall j absorbed in wall i. $D_{i,j,k}$ are tabulated in Table 5 for cavities C_1, C_2, and C_3. The net radiative heat transfer rate to surface i is given by

$$Q_{\mathrm{rad},i} = \sum_{\mathrm{band}:k} \sum_{\mathrm{surface}:j} A_j \varepsilon_{k,j} \sigma T_j^4 F_k(T_j) D_{j,i,k} - A_i \sigma T_i^4 \sum_{\mathrm{band}:k} \varepsilon_{k,i} F_k(T_i) + \sum_{\mathrm{band}:k} H_{i,k} Q_{\mathrm{sol},k}, \quad (10)$$

where $H_{i,k}$ is the fraction of solar energy in band k absorbed in wall i, calculated using MC for uniformly distributed and diffuse radiation incident on the aperture plane. Eq. (10) is used to compute the term $Q_{\mathrm{rad},s}$ in Eq. (2) and $Q_{\mathrm{rad},p}$ in Eq. (3). Note that radiation heat transfer within the gas is omitted from consideration since the gas inside the volume is treated as a non-participating medium.

Convection—Empirical correlations are applied for calculating convection heat transfer. Table 2 lists the flow type, the correlation, their references, and the reservoir pairs for which the correlation is applied to calculate the heat transfer coefficient. Thus,

$$Q_{\mathrm{conv},i\to j} = A_{i,j} \bar{h}_{\mathrm{conv},i,j} (T_i - T_j). \quad (11)$$

Conduction—Linear temperature profiles are assumed inside individual solids. While this is a reasonable approximation for steady-state conditions, conduction heat transfer may be underestimated during transients, especially for the ceramic insulation, and can be overcome by further subdividing each ceramic segment in the radial direction. Nevertheless, since conduction plays a secondary role in the transport of heat, no further detailed analysis was implemented in this study. Thus, conduction heat transfer between two solids is

Please cite this article as: Petrasch, J., Steinfeld, A., Dynamics of a solar thermochemical reactor for steam-reforming of methane. Chemical Engineering Science (2007), doi: 10.1016/j.ces.2007.04.036

approximated as

$$Q_{\text{cond},s1\to s2} = A_{s1,s2}\frac{k_{s1}}{l_{s1\to \text{if}}}(T_{s1} - T_{\text{if}}) = A_{s1,s2}\frac{k_{s2}}{l_{s2\to \text{if}}}(T_{\text{if}} - T_{s2}), \quad (12)$$

where

$$T_{\text{if}} = \frac{T_{s1}k_{s1}/l_{s1\to \text{if}} + T_{s2}k_{s2}/l_{s2\to \text{if}}}{k_{s1}/l_{s1\to \text{if}} + k_{s2}/l_{s2\to \text{if}}}. \quad (13)$$

Thermal conductivities k are evaluated at $(T_{s1} + T_{\text{if}})/2$. References to thermal conductivity data for relevant solid materials are found in Table 4. Conduction lengths $l_{i\to \text{if}}$ are tabulated in Table 3.

(d) *Implementation*: The model is numerically implemented using MATLAB-Simulink. Viscosity of relevant gases (H_2, CO, CO_2, CH_4, H_2O, N_2, and O_2) is calculated using relations from VDI (1984). Thermal conductivities of gases are calculated using polynomial fits of data from VDI (1984) and Incropera and DeWitt (1996). Thermodynamic properties of pure gases and mixtures are calculated using Cantera (Goodwin, 2003) and NASA CET-85 (Gordon and McBride, 1971) programs, based on polynomial coefficients presented in McBride et al. (1993). Thermal conductivities and specific heat of solids are calculated using polynomial approximations based on data from various sources listed in Table 4. A 4th order Runge–Kutta time integration scheme using a fixed time step of 0.05 s has been used.

3. Modeling results

The following operation modes are simulated: (1) purging with inert gas; (2) thermal testing by heating the reactor without chemical reaction; (3) experimental run by heating, addition of steam, addition of methane, chemical reaction, and shutdown; and (4) Cycling testing by 3-day 8-h/day operation with daily startups and shutdowns.

(1) *Purging*—The solar reactor, initially filled with air, is purged with pure N_2 at a mass flow rate of 200 kg/h (2 mol/s). Total system pressure is 8 bar. Fig. 4 shows the variation of the outlet gas composition with time, with 75% recirculation (solid curve) and without recirculation (dotted curve). The purging effect is stronger initially with recirculation because of the higher internal mass flow, but convergence to the steady state is slower due to mixing.

(2) *Thermal testing*—The solar reactor is subjected to heating under the following conditions: $T_0 = 300$ K, $p = 8$ bar, inflow = 2 mol N_2/s, recirculated mass-flow equals 3 times inflow, $Q_{\text{solar}} = 0$ for $0\text{ s} \leqslant t < 100$ s, and $Q_{\text{solar}} = 2.05 \times 10^5$ W for $100\text{ s} \leqslant t < 1000$ s. The net radiative transfer rates, the temperatures of selected reactor components, the flow rates of the inflow/outflow, and the efficiency are shown in Fig. 5 (a), (b), (c), and (d), respectively. Most of the radiation is transferred to the porous absorbers P_1 and P_2 during the initial seconds

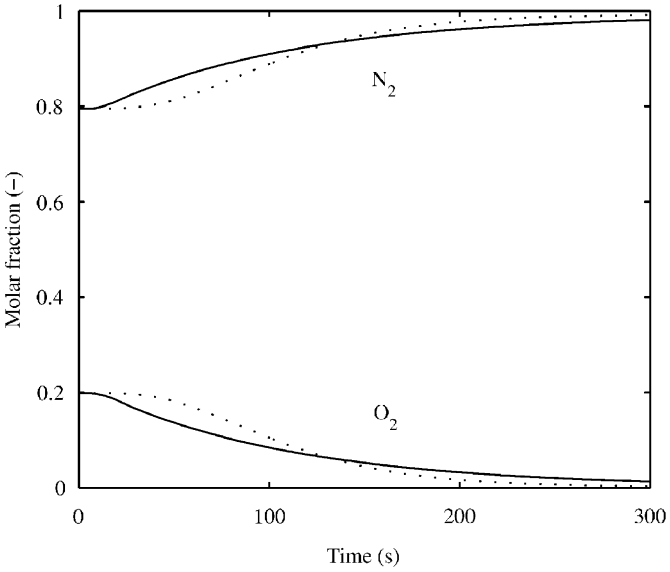

Fig. 4. Outlet chemical composition for purging of reactor at $T_0 = 300$ K, $p = 8$ bar, $\dot{m} = 200$ kg N_2/h, with three-fold recirculation (solid curve) and without recirculation (dotted curve).

of heating. As their temperature increases, the net radiative transfer rate decreases because of re-radiation to other system components. Notably, heat transfer to the quartz window (Fig. 5a, curve Q) picks up only after the absorbers have reached temperatures above 800 K (Fig. 5b, curves P_1 and P_2). This is because the window is heated mainly by radiation emitted from inside the reactor since the absorptance of the window approaches zero in the visible band but is relatively high in the IR band (see Fig. 3, B and 3). The temperature of the quartz window is plotted in Fig. 5b, curve Q. The sum of the radiative transfer rates to the reactor components decreases over time as less energy is stored as sensible heat (Table 5). The sharp peak of the outlet mass flow rate after 100 s is due to the rapid thermal expansion of the gas inside the reactor, while the inlet mass flow rate is held constant. Instantaneous energy efficiency for the solar chemical reactor is defined as

$$\eta_{\text{en}} = \frac{\dot{m}_{\text{out}}h_{\text{out}} - \dot{m}_{\text{in}}h_{\text{in}}}{Q_{\text{solar}}}. \quad (14)$$

Eq. (14) is sufficient for describing the performance of solar system operating in steady state and equal inflow/outflow rates. However, switching from one inlet composition to another may lead to efficiencies greater than 1 or negative efficiencies depending on the enthalpy of the inlet and outlet streams. Thus, for transients, the overall efficiency is defined as

$$\eta_{\text{en,ov}} = \frac{\int_0^t (\dot{m}_{\text{out}}h_{\text{out}} - \dot{m}_{\text{in}}h_{\text{in}})\,\mathrm{d}t^*}{\int_0^t Q_{\text{solar}}\,\mathrm{d}t^*}. \quad (15)$$

The efficiency is undefined for $t < 100$ s since the denominators of Eqs. (14)–(15) are zero. As the reactor is heated, the

Please cite this article as: Petrasch, J., Steinfeld, A., Dynamics of a solar thermochemical reactor for steam-reforming of methane. Chemical Engineering Science (2007), doi: 10.1016/j.ces.2007.04.036

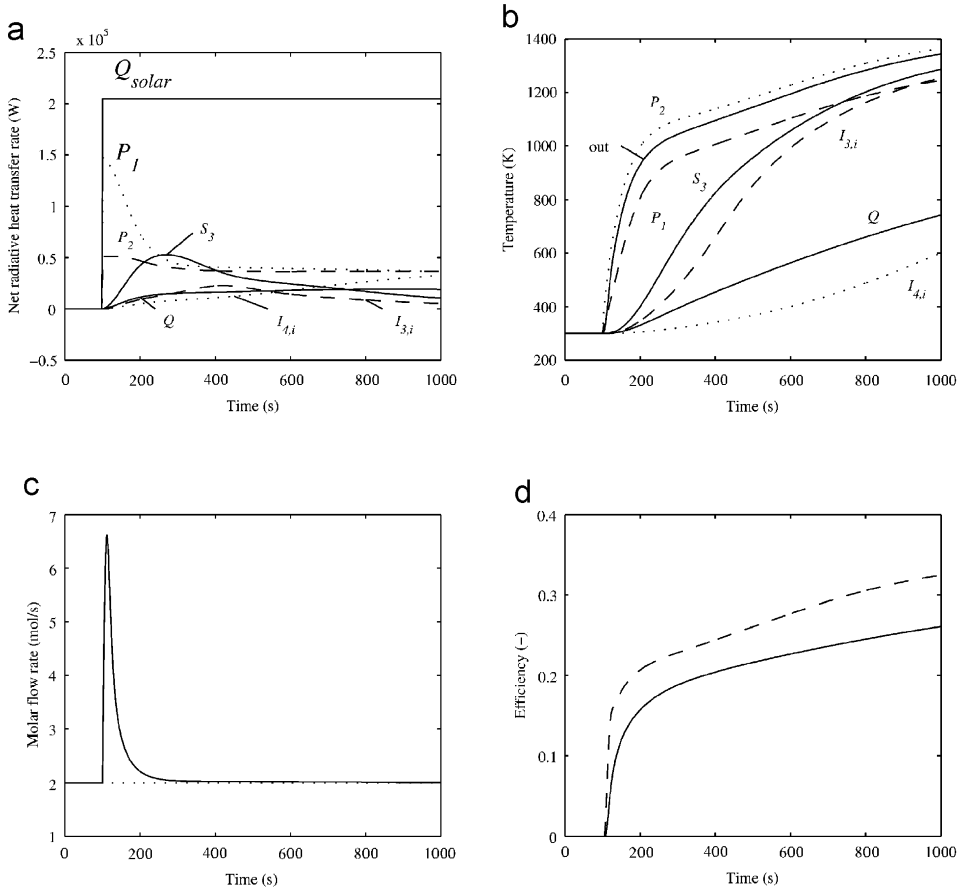

Fig. 5. Step response to solar heating rate of $Q_{\text{solar}} = 2 \times 10^5$ W at $t = 100$ s, $\dot{n} = 2$ mol N_2/s and $p = 8$ bar. (a) net radiative transfer; (b) temperature of system components; (c) molar flow rates of inflow (dotted curve) and outflow (solid curve); and (d) energy efficiency η_{en} (dashed curve), overall energy efficiency $\eta_{\text{en,ov}}$ (solid curve).

efficiencies are relatively low since a significant fraction of the solar energy is transferred to the solid components. The overall efficiency is lower than its instantaneous counterpart because energy is stored in the walls during heating. The instantaneous efficiency is only influenced by the instantaneous rate of energy storage whereas the overall efficiency contains information on the reactor's history of energy storage.

(3) *Experimental run*—A representative solar reforming experimental run is shown in Fig. 6. It consists of heating with $Q_{\text{solar}} = 205$ kW under inert atmosphere (N_2) during $100\text{ s} < t \leqslant 1000\text{ s}$, followed by injection of steam during $1000\text{ s} < t \leqslant 1500\text{ s}$. At $t = 1500$ s, CH_4 is added to the inlet flow at a H_2O:CH_4 molar ratio 2.7, while simultaneously increasing the solar input power to $Q_{\text{solar}} = 410$ kW for $1500\text{ s} < t \leqslant 3500\text{ s}$. At $t = 3500$ s, the experiment is shut down by stopping the input of solar power.

As expected from results of the thermal testing, the largest portion of radiative energy is transferred to the porous absorbers, and from there to the reacting flow. Temperatures rise quickly while heating under N_2, and drops to a quasi steady-state level once H_2O is inserted as a result of its higher mass flow rate and specific heat. When CH_4 feed is started, temperatures fall again in spite of the increase in the solar input power because of the highly endothermic reforming reaction. Steady-state conditions are not reached during operation. However, since the heat transfer through the insulation components is low compared to the overall heat transfer, quasi-steady state is reached for the window, porous absorber, and inner reactor walls. The outlet temperature approaches a constant value of 1077 K, which is consistent with the steady-state modeling value of 1077 K, and with the experimentally measured value of 1018 K, both reported by Petrasch et al. (2005). For an optimal heating strategy, the temperature overshoot during $500\text{ s} < t < 1700\text{ s}$ should be avoided, either by switching earlier to H_2O and CH_4, or by reducing the initial Q_{solar}. The outlet molar flow rate exhibits a sharp peak during the rapid heating due to thermal expansion, and is higher than inlet flow rate during the chemical reaction due to the formation of syngas. At $t = 3500$ s, there is a sharp drop in the outlet molar flow rate as the chemical reaction ceases. The overall energy efficiency increases during the cooling phases at $t = 1000$, 1500, and 3500 s, because the sensible heat stored in the reactor components is transferred to the reactants. Efficiencies further rise during the chemical reaction phase, approaching steady-state values of about 0.85. The instantaneous efficiency is undefined (set to zero) when Q_{solar} equals zero. Furthermore, when

Please cite this article as: Petrasch, J., Steinfeld, A., Dynamics of a solar thermochemical reactor for steam-reforming of methane. Chemical Engineering Science (2007), doi: 10.1016/j.ces.2007.04.036

Table 5
Radiation transfer parameters for cavities C_1, C_2, and C_3

Cavity C_1				
$D_{i,j,1}$	P_1	P_2	Q	I_4
P_1	0.1010	0.2600	0.4960	0.1430
P_2	0.1030	0.4660	0.3870	0.0430
Q	0.1590	0.3140	0.2520	0.0210
I_4	0.4480	0.3420	0.2070	0.0030
$D_{i,j,2}$				
P_1	0.2170	0.4600	0	0.1220
P_2	0.1820	0.5360	0	0.0520
Q	0.2630	0.4440	0	0.0300
I_4	0.4760	0.5110	0	0.0030
$D_{i,j,3}$				
P_1	0.1290	0.3000	0.4250	0.0720
P_2	0.1190	0.4680	0.3070	0.0230
Q	0.2000	0.3650	0.1790	0.0150
I_4	0.4470	0.3560	0.1940	0.0010
A_{rad} (m^2)	0.4000	1.0110	1.3930	0.1250
H_{b1}	0	0	0.9790	0
H_{b2}	0.25	0.721	0	0.003
H_{b3}	0.0920	0.2610	0.6370	0
ε_{b1}	0.9750	0.9750	0.8730	1.0
ε_{b2}	0.9750	0.9750	0	0.8
ε_{b3}	0.9750	0.9750	0.5960	0.5

Cavity C_2						
$D_{i,j,1}$	I_{4i}	I_{3i}	I_{2i}	S_2	S_3	P_1
I_{4i}	0	0.5170	0.0020	0	0.1210	0.3600
I_{3i}	0.0380	0.0600	0.0750	0.1010	0.6330	0.0930
I_{2i}	0	0.2480	0.0690	0.6820	0.0010	0
S_2	0	0.3110	0.6400	0.0490	0	0
S_3	0.0140	0.9670	0	0	0	0.0190
P_1	0.2000	0.7040	0	0	0.0960	0
$D_{i,j,2}$						
I_{4i}	0.0400	0.4840	0.0020	0	0.1310	0.3430
I_{3i}	0.0360	0.1820	0.0750	0.0930	0.5320	0.0820
I_{2i}	0.0010	0.2470	0.1490	0.5940	0.0090	0
S_2	0	0.2870	0.5590	0.1500	0.0040	0
S_3	0.0150	0.8130	0.0040	0.0020	0.1440	0.0220
P_1	0.1900	0.6160	0	0	0.1080	0.0860
$D_{i,j,3}$						
I_{4i}	0.0870	0.4480	0.0030	0.0010	0.1470	0.3140
I_{3i}	0.0330	0.3080	0.0760	0.0860	0.4290	0.0680
I_{2i}	0.0010	0.2490	0.2370	0.4910	0.0220	0
S_2	0	0.2650	0.4620	0.2590	0.0140	0
S_3	0.0160	0.6550	0.0100	0.0070	0.2860	0.0260
P_1	0.1740	0.5180	0	0	0.1270	0.1810
A_{rad} (m^2)	0.1980	2.6980	0.8190	0.8730	1.7680	0.3570
ε_{b1}	1.0	1.0	1.0	1.0	1.0	0.9750
ε_{b2}	0.8	0.8	0.8	0.8	0.8	0.9750
ε_{b3}	0.5	0.5	0.5	0.5	0.5	0.9750

Cavity C_3			
$D_{i,j,1}$	S_3	S_2	P_2
S_3	0.2090	0.2200	0.5710
S_2	0.4770	0.1210	0.4020
P_2	0.7540	0.2460	0

Table 5 (*Continued*)

Cavity C_3			
$D_{i,j,1}$	S_3	S_2	P_2
$D_{i,j,2}$			
S_3	0.1990	0.1900	0.6110
S_2	0.4120	0.1210	0.4670
P_2	0.6450	0.2290	0.1260
$D_{i,j,3}$			
S_3	0.1650	0.1380	0.6970
S_2	0.2990	0.1050	0.5960
P_2	0.4610	0.1820	0.3570
A_{rad} (m^2)	1.6310	0.7550	1.2620
ε_{b1}	1.0	1.0	0.9750
ε_{b2}	0.8	0.8	0.9750
ε_{b3}	0.5	0.5	0.9750

switching from one feedstock to a different one, efficiencies above 1 can be obtained as the absolute enthalpy of the inlet feedstock is below the absolute enthalpy of the previous feedstock still present in the reactor. This shows that the use of the instantaneous efficiency as an indicator of the reactor's performance can be misleading for a solar chemical reactors in transient operation.

(4) *Cyclical testing*—In contrast to conventional chemical reactors, a solar chemical reactor is constantly subjected to varying input parameters, especially Q_{solar}. Even under favorable weather conditions, the reactor undergoes shutdown and restart on a daily basis. Three consecutive days of operation are simulated, assuming 8 h of daily operation at 400 kW followed by 16 h without solar radiation. Fig. 7 shows the results of the 3-day cyclical operation for: (a) net-radiative heat transfer rates; (b) component temperatures; (c) inlet gas chemical compositions; (d) outlet gas chemical composition; (e) molar in- and out-flow rates; (f) overall efficiency; (g) temperature of insulation components; and (h) net heat flow rate to insulation components. Rapid heating and shutdown of the main components P_1 and P_2 can be observed, which is crucial for non-continuous operation. Quasi-steady state is attained quickly and, thus, good quality products are yielded for most of the operational time. The quasi-steady efficiency of 0.85 is approached after 3 h of operation of the first day. Afterwards, the overall efficiency only varies slightly, although dents may be observed during daily heating. As far as the temperature and heat flow to the ceramic insulation components are concerned, steady state is not attained because of their large time constants; however, quasi periodic-oscillation is reached after only one cycle.

4. Experimental validation

A representative solar experimental run, performed at the solar tower facility of the Weizmann Institute of Science (Israel), serves as the basis for comparing model and experimental results. The input data is shown in Fig. 8: (a)

Please cite this article as: Petrasch, J., Steinfeld, A., Dynamics of a solar thermochemical reactor for steam-reforming of methane. Chemical Engineering Science (2007), doi: 10.1016/j.ces.2007.04.036

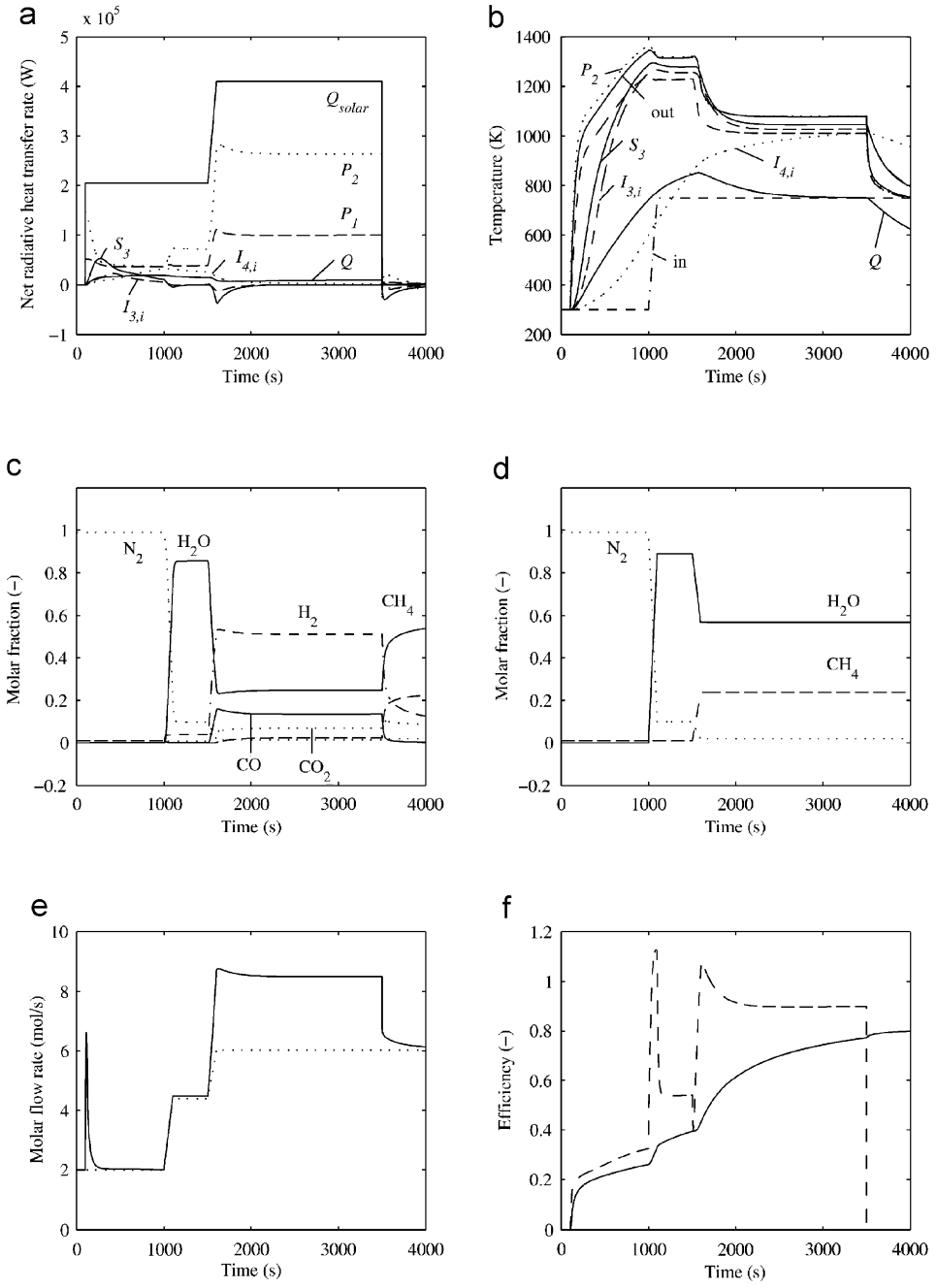

Fig. 6. Representative solar reforming experiment consisting of heating under inert atmosphere (N_2) during $100\,s < t \leqslant 1000\,s$, followed by injection of steam during $1000\,s < t \leqslant 1500\,s$, addition of CH_4 to the inlet flow at a H_2O-CH_4 molar ratio 2.7, while simultaneously increasing the solar input power to $Q_{solar} = 410\,kW$ for $1500\,s < t \leqslant 3500\,s$, and finally shutdown by stopping the input of solar power at $t = 3500\,s$. (a) net radiative heat transfer rate to reactor; (b) temperature of reactor components; (c) inlet molar composition; (d) outlet molar composition; (e) total molar flow rate at reactor inlet (dotted curve) and outlet (solid curve); and (f) instantaneous (dashed) and overall (solid) energy efficiency.

input gas temperature and molar flow rates; (b) input gas composition; and (c) input solar power. The input flow rates were obtained from steam and feedstock flow-rate settings. The input gas composition to the solar reactor was assumed to be the equilibrium composition at the exit conditions of the pre-reformer (Petrasch et al., 2005). The input solar power to the reactor has been calculated for the heliostat field configuration applied during the experiment and weighted by the measured incident normal solar radiation. In this experimental run, the solar reactor was heated under a flow of steam for 5000 s, while the solar power input was adjusted to reach an approximate steady-state outlet gas temperature of 1000 K. Afterwards, the reactor was subjected to the reacting flow—a mixture of H_2O, CH_4, H_2, and CO_2 obtained at the exit of the pre-reformer—while the solar power input was increased to compensate for the energy consumption by the endothermic

Please cite this article as: Petrasch, J., Steinfeld, A., Dynamics of a solar thermochemical reactor for steam-reforming of methane. Chemical Engineering Science (2007), doi: 10.1016/j.ces.2007.04.036

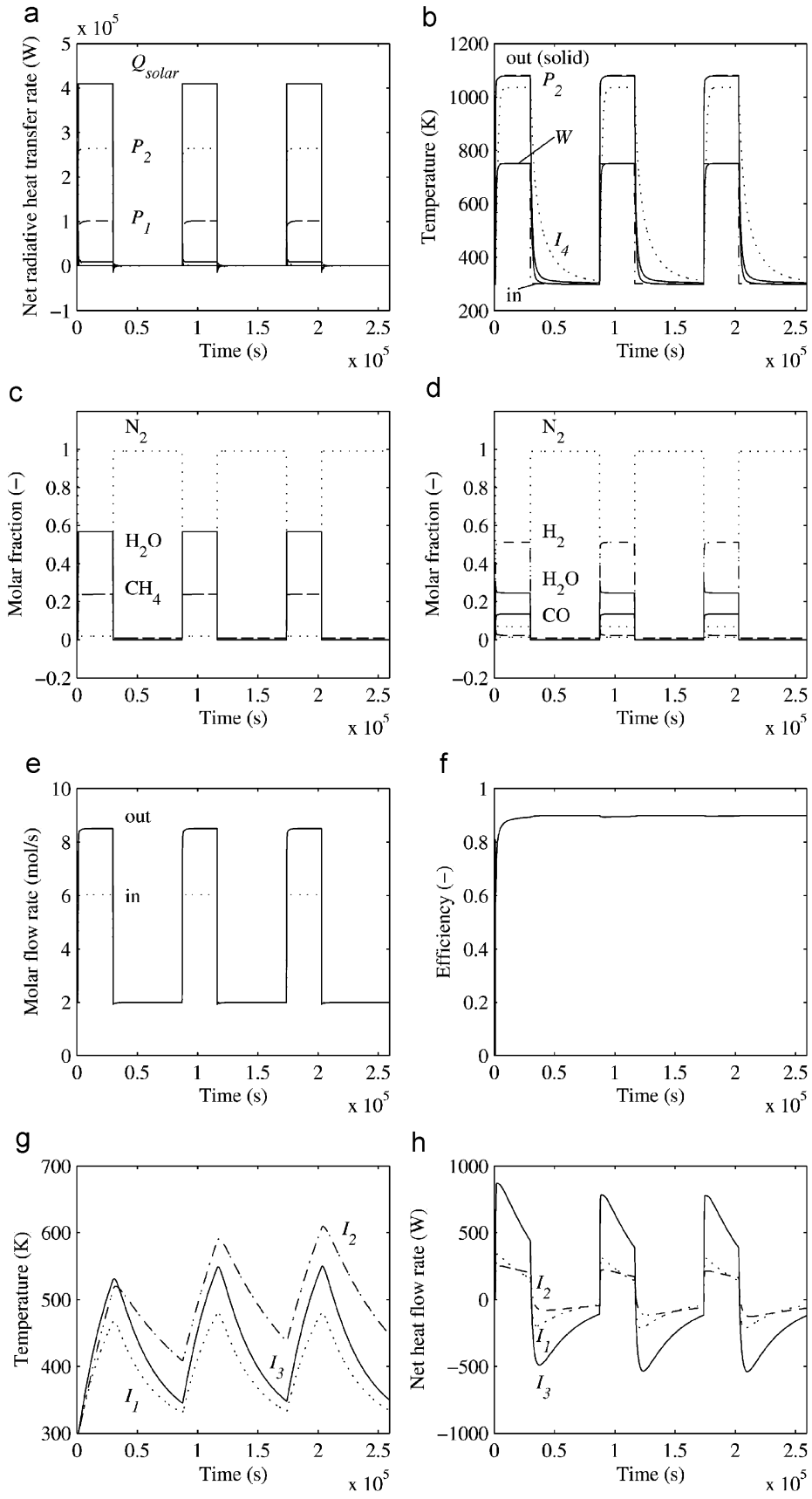

Fig. 7. Three-day cyclical operation: (a) net-radiative heat transfer rates; (b) component temperatures; (c) inlet chemical compositions; (d) outlet chemical composition; (e) molar in- and out-flow rates; (f) overall efficiency; (g) temperature of insulation components; and (h) net heat flow rate to insulation components.

Please cite this article as: Petrasch, J., Steinfeld, A., Dynamics of a solar thermochemical reactor for steam-reforming of methane. Chemical Engineering Science (2007), doi: 10.1016/j.ces.2007.04.036

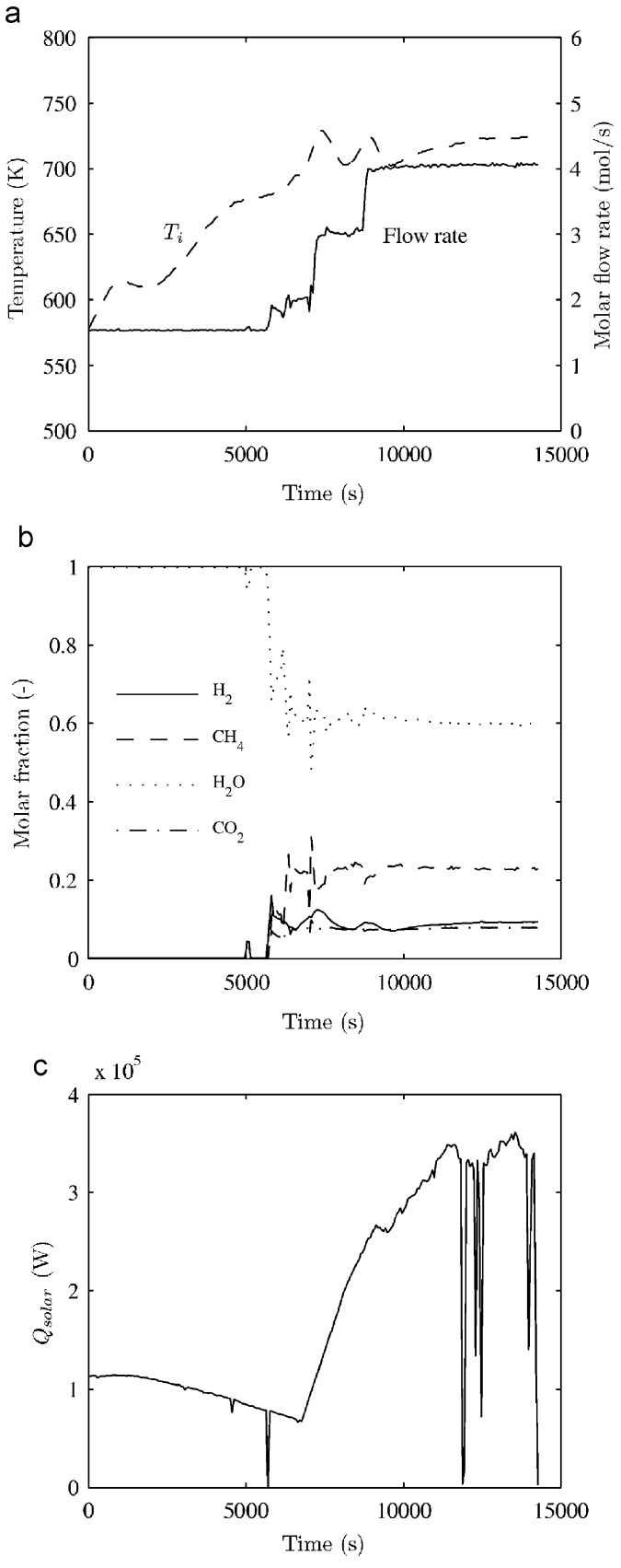

Fig. 8. Input data for validation case: (a) temperature and molar flow rate of gas entering the receiver; (b) chemical composition of input gas to the receiver; and (c) solar power input to reactor.

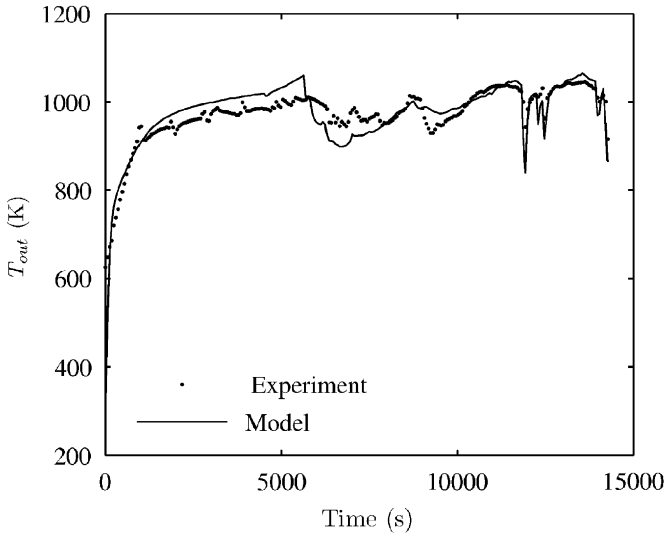

Fig. 9. Gas outlet temperature model vs. experiment.

transformation. The numerically modeled and experimentally measured temperature of the outgoing gases at the solar reactor exit is shown in Fig. 9. The agreement is reasonably good. The temperature drops correspond to solar power fluctuations due to passing clouds (see Fig. 8c). For situations where steady state is approached (for example, after 4000 s), the model predicts slightly higher values than those measured, partly because of the non-ideal behavior of the optical system (e.g. combined effect of the heliostat field and CPC secondary concentrator) and because of the complex radiation/convection/conduction heat transfer in the solar reactor. Further inaccuracies are attributed to the thermal inertia of the measurement devices for temperature, flow, and gas compositions, sampled only every 60 s.

5. Conclusion

We have developed a non-linear dynamic simulation model for a solar reforming reactor that is able to predict temperatures, heat transfer rates, outlet mass flow rates, and product composition during purging, thermal testing, experimental run, and cycling operation. Time constants of relevant components vary between 2 s for species transport in reactor volumes and 1×10^5 s for thermal energy in insulation. Quasi-steady-state values for outlet temperatures are consistent with those obtained by steady-state modeling and with those measured experimentally. Heating by concentrated solar radiation allows for quick startup while keeping stable dynamic behavior. The reactor's overall efficiency varies strongly during initial operation phases because sensible heat is transferred to and removed from the reactor components during heating and cooling phases, respectively. A reduction of the thermal mass of the reactor, especially of insulation components, should result in an increase in the reactor efficiency and performance. Furthermore, reduced thermal mass leads to shorter time constants, thus enhancing the reactors response time to changes in solar irradiation. This

Please cite this article as: Petrasch, J., Steinfeld, A., Dynamics of a solar thermochemical reactor for steam-reforming of methane. Chemical Engineering Science (2007), doi: 10.1016/j.ces.2007.04.036

approach, however, requires a tight control of the inlet mass flow rate.

Acknowledgments

This work has been conducted in the framework of the EU-Project SOLREF, funded by the European Commissions under contract no. SES6-CT-2004-502829 SOLREF. We thank M. Epstein from the Weizmann Institute of Science and S. Moeller from DLR-German Space Agency for providing the solar experimental data.

References

Al-Nimr, M.A., Damseh, R.A., 1998. Dynamic behaviour of baffled solar air heaters. Renewable Energy 13, 153–163.

Arinze, E.A., Schoenau, G.J., Sokhansanj, S., Adefila, S.S., Mumah, S.M., 1993. A dynamic performance simulation model of flat-plate solar collectors for a heat pump system. Energy Conversion and Management 34, 33–49.

Beckhaus, P., Heinzel, A., Mathiak, J., Roes, J., 2004. Dynamics of H_2 production by steam reforming. Journal of Power Sources 127, 294–299.

Bequette, B.W., 1998. Process Dynamics Modeling, Analysis and Simulation. Prentice-Hall, Englewood Cliffs, NJ.

Bequette, B.W., 2003. Process Control Modeling, Design and Simulation. Prentice-Hall, Englewood Cliffs, NJ.

Buck, R., 2002. Massenstrom-Instabilitäten bei volumetrischen Receiver-Reaktoren. Fortschritt-Berichte VDI, Reihe 3 Verfahrenstechnik.

Buck, R., Muir, R.E., Hogan, E.H., Skocypec, R.D., 1991. Carbon dioxide reforming of methane in a solar volumetric receiver/reactor: the CAESAR project. Solar Energy Materials 24, 449–463.

Buck, R., Abele, M., Bauer, H., Seitz, A., Tamme, R., 1994. Development of a volumetric receiver-reactor for solar methane reforming. ASME—Journal of Solar Energy Engineering 116, 449.

Buzás, J., Farkas, I., Biró, A., Németh, R., 1998. Modelling and simulation of a solar thermal system. Mathematics and Computers in Simulation 48, 33–46.

Chaabene, M., Annabi, M., 1997. A dynamic model for predicting solar plant performance and optimum control. Energy 22, 567–578.

Cui, H., Hou, X., Yuan, X., 2003. Energy analysis of space solar dynamic heat receivers. Solar Energy 74, 303–308.

Dahl, J.K., Weimer, A.W., Lewandowski, A., Bingham, C., Bruetsch, F., Steinfeld, A., 2004. Dry reforming of methane using a solar-thermal aerosol flow reactor. Industrial & Engineering Chemistry Research 43, 5489–5495.

De Ron, A.J., 1980. Dynamic modeling and verification of a flat-plate solar collector. Solar Energy 24, 117–128.

Epstein, M., Spiewak, I., 1996. Solar experiments with a tubular reformer. In: Proceedings of the 8th International Symposium on Solar Thermal Concentrating Technologies, Cologne, Germany, Müller, Heidelberg, pp. 1209–1229.

Gokon, N., Oku, Y., Kaneko, H., Tamaura, Y., 2002. Methane reforming with CO_2 in molten salt using FeO catalyst. Solar Energy 72, 243–250.

Goodwin, D.G., 2003. An Open-Source, Extensible software suite for CVD process imulation. In: Allendorf, M., Maury, F., Teyssandier, F. (Eds.), Chemical Vapor Deposition XVI and EUROCVD 14, ECS Proceedings, vol. 2003-08. The Electrochemical Society, pp. 155–162.

Gordon, S., McBride, B.J., 1971. Computer Program for Calculation of Complex Chemical Equilibrium Composition, Rocket Performance, Incident and Reflected Shocks and Chapman–Jouguet Detonations. NASA Report SP-273.

Guzzella, L., 2001. System dynamics. Lecture notes, ETH-Zurich.

Hashish, M.A., El-Refaie, M.F., 1983. Reduced order dynamic model of the flat-plate solar collector. Applied Mathematical Modelling 7.

Hogan Jr., R.E., Skocypec, R.D., Diver, R.B., Fish, J.D., Garrait, M., Richardson, J.T., 1990. A direct absorber reactor/receiver for solar thermal applications. Chemical Engineering Science 45, 2751–2758.

Incropera, F.P., DeWitt, D.P., 1996. Introduction to Heat Transfer. Wiley, New York.

Jallut, C., Jemni, A., Lallemand, M., 1988. Steady-state and dynamic characterization of an array of flat-plate collectors. Solar & Wind Technology 5, 573–579.

Kaushik, S., Sheridan, N., Lam, K., Kaul, S., 1985. Dynamic simulation of an ammonia-water absorption cycle solar heat pump with integral refrigerant storage. Heat Recovery Systems 5, 101–116.

Kaushik, S., Rao, S., Kumari, R., 1991. Dynamic simulation of an aqua-ammonia absorption cooling system with refrigerant storage. Energy Conversion and Management 32, 197–206.

Kodama, T., Koyanagi, T., Shimizu, T., Kitayama, Y., 2001. CO_2 reforming of methane in a molten carbonate salt for use in solar thermochemical processes. Energy & Fuels 15, 60–65.

Levy, M., Rosin, H., Levitan, R., 1989. Chemical reactions in a solar furnace by direct irradiation of the catalyst. ASME—Journal Solar Energy Engineering 111, 96–97.

Levy, M., Rubin, R., Rosin, H., Levitan, R., 1992. Methane reforming by direct solar irradiation of the catalyst. Solar Energy 17, 749–756.

Lucks, C.F., Matolich J., Van Valzor, J.A., 1954. USAF TR 6145, pp. 1–71.

Lucks, C.F., Deem, H.W., Wood, W.D., 1960. American Ceramic Society Bulletin 39, p. 313.

Luyben, W.L., 1989. Process Modeling Simulation and Control for Chemical Engineers. second ed. McGraw-Hill, New York.

Maffezzoni, C., Parigi, F., 1982a. Dynamic analysis and control of a solar power plant—I. Dynamic analysis and operation criteria. Solar Energy 28, 105–116.

Maffezzoni, C., Parigi, F., 1982b. Dynamic analysis and control of a solar power plant—II. Control system design and simulation. Solar Energy 28, 117–128.

Mahan, J.R., 2002. Radiation Heat Transfer: A Statistical Approach. Wiley, New York.

McBride, B.J., Gordon, S., Reno, M.A., 1993. Coefficients for calculating thermodynamic and transport properties of individual species. NASA Report TM-4513.

Microtherm International Limited, 2005. Microtherm insulation product and performance data brochure, ⟨http://www.microtherm.uk.com⟩.

Moeller, S., Buck, R., Tamme, R., Epstein, M., Liebermann, D., Moshe, M., Fisher, U., Rotstein, A., Sugarmen, C., 2002. Solar production of syngas for electricity generation: SOLASYS project test-phase. In: Steinfeld, A. (Ed.), Proceedings of the 11th SolarPACES International Symposium on Concentrated Solar Power and Chemical Energy Technologies, Zurich, Switzerland pp. 231–237.

Palik, E.D., 1985. Handbook of Optical Constants of Solids. Academic Press, New York.

Petrasch, J., Moeller, S., Steinfeld, A., 2005. Solar steam reforming of hydrocarbons—thermodynamic analysis and process simulation. In: Proceedings of the 2005 ECOS conference, Trondheim, Norway.

Ray, A., 1980. Dynamic modelling of once-through subcritical steam generator for solar applications. Applied Mathematical Modelling 4.

Ray, A., 1981. Nonlinear dynamic model of a solar steam generator. Solar Energy 26, 297–306.

Richardson, J.T., Paripatyadar, S.A., 1990. Carbon dioxide reforming of methane with supported rhodium. Applied Catalysis 61, 293–309.

Robbins, F.A., Zhu, H., Jackson, G.S., 2003. Transient modeling of combined combistin/CH_4 steam reforming. Catalysis Today 83, 141–156.

Scott, R.B., 1962. Cryogenic Engineering. Van Nostrand, Princeton, NJ, p. 329.

Special Metals Corporation, 2000. Product Reference Guide, Special Metals Corporation, Huntington, WV.

Steinfeld, A., 2005. Solar thermochemical production of hydrogen—a review. Solar Energy 78 (5), 603–615.

Tamme, R., Buck, R., Epstein, M., Fisher, U., Sugarmen, C., 2001. Solar upgrading of fuels for generation of electricity. Journal of Solar Energy Engineering 123, 160–163.

Please cite this article as: Petrasch, J., Steinfeld, A., Dynamics of a solar thermochemical reactor for steam-reforming of methane. Chemical Engineering Science (2007), doi: 10.1016/j.ces.2007.04.036

Touloukian, Y.S., Powell, R.W., Ho, C.Y., Klemens, P.G., 1970. Thermophysical Properties of Matter. IFI, Plenum, New York.

TRNSYS—A transient system simulation program, Version 16, © 2005 Solar energy laboratory, University of Wisconsin—Madison, ⟨ http://sel.me.wisc.edu/trnsys/⟩.

Van Lack, L.H., 1964. Physical Ceramics for Engineers. Addison-Wesley, Reading, MA, p. 146.

VDI, 1984. VDI-Wärmeatlas, Berechnungsblätter für den Wärmeübergang 4., neubearbeitete und erweiterte Auflage, VDI-Verlag GmbH, Düsseldorf.

Wood, W.D., Deem, H.W., Lucks, C.F., 1964. Thermal Radiative Properties. Plenum Press, New York.

Wörner, A., Tamme, R., 1998. CO_2 reforming of methane in a solar driven volumetric receiver-reactor. Catalysis Today 46, 165–174.

Yang, W., Taniguchi, H., Kudo, K., 1995. Radiative Heat Transfer by the Monte Carlo Method. Advances in Heat Transfer vol. 27, Academic Press, New York.

Please cite this article as: Petrasch, J., Steinfeld, A., Dynamics of a solar thermochemical reactor for steam-reforming of methane. Chemical Engineering Science (2007), doi: 10.1016/j.ces.2007.04.036